Diamond & Related Materials 86 (2018) 1–7

Contents lists available at ScienceDirect

Diamond & Related Materials

journal homepage: www.elsevier.com/locate/diamond

Ex-vivo studies on friction behaviour of ureteral stent coated with Ag clusters incorporated in a:C matrix

Isabel Carvalho[a,b,*], Mostafa Faraji[a], Amílcar Ramalho[a], António P. Carvalho[c], Sandra Carvalho[a,d], Albano Cavaleiro[a,b]

[a] SEG-CEMMPRE Mechanical Engineering Department, University of Coimbra, 3030-788 Coimbra, Portugal
[b] IPN-LED&MAT Instituto Pedro Nunes, Laboratory for Wear, Testing & Materials, Rua Pedro Nunes, 3030-199 Coimbra, Portugal
[c] Trofa Saúde Hospital, Rua do Raio, 4710-923 Braga, Portugal
[d] CFUM-UP, University of Minho, Campus de Azurém, 4800-058 Guimarães, Portugal

ARTICLE INFO

Keywords:
Ag/a:C
Inert gas condensation
Friction
Ureteral stent

ABSTRACT

Coated ureteral stents must be placed in the human body without hurting the body tissue and, simultaneously, support the application without degrading the top active layer. In this work Ag clusters incorporated in a:C (Ag/a:C) matrix were produced by plasma gas condensation process. After optimizing some deposition parameters, as cluster source pressure and power density, two different clusters sizes were obtained 11 ± 2 nm using cluster source pressure of 100 Pa, and a bimodal size using cluster source pressure of 200 Pa (31 ± 22 nm and 260 ± 135 nm). Ag/a:C coatings showed a total adhesion to substrate, without delamination of the film, even after a month of immersion in distilled water. The friction coefficient of the coatings and the uncoated reference were determined and show a reduction from 0.22 for the reference stent to 0.12 for the Ag/a:C coated stents produced at 100 Pa and to 0.16 for the Ag/a:C coated stents produced at 200 Pa.

1. Introduction

Intubation of the lower urinary system has been used throughout the recorded history of medicine, for treatment of obstruction, and the use of catheters, urethral and ureteral stents in the treatment of urinary tract diseases has become integral part of contemporary urologic practice. However, they frequently are associated with significant patient discomfort (pain, urgency, frequency) and common complications including microbial colonization (encrustation and infection) [1,2]. In fact, any catheter material placed in the urinary tract, such as indwelling transurethral catheters and ureteral stents, provides a surface for bacterial colonization which is susceptible to the formation of a persistent bacterial biofilm with increasing indwelling time [3]. The importance of these limitations is that they are not only troubles to the patient but can lead to significant morbidity, urinary retention, ureteral damage, recurrent infections [2].

In most cases, when these problems occur, the total replacement of the biomaterial is essential to successfully treat the patient, which represents a huge economic burden for the healthcare system and, above of all, a significant discomfort to the patient [4]. In an attempt to solve these problems and prevent such morbidity, over the past several decades great efforts have been dedicated to modifying the stent itself and to the development of antibacterial materials and new concepts able to prolong the medical devices lifetime. These strategies include changes to device design, polymeric composition, drug eluting, surface coatings and nanotechnology approaches [2,5–7]. Of these, drug-eluting and surface coatings (DLC coatings and Heparin coatings) represent some of the innovative concepts in the field of urologic stents which are the most studied and display the most promise for advancing ureteral stent use and efficacy [2,3,6,8].

Heparin coatings were first proposed three decades ago for vascular stent applications, and presently they are used in ureteral stents to inhibit the bacterial adhesion. However, some reports state that heparin coatings favour the adhesion of bacteria present in the urinary tract system [2,8,9], leading to a worse final performance when comparing with conventional silicone stents. DLC coatings are claimed to reduce the friction coefficient of stent surface, improving the patients comfort; nevertheless, although they enhance the corrosion resistance and reduce the risk of encrustation, their performance is still far from what should be desired [2,3]. Moreover, previous studies have shown that the DLC coatings do not show any antibacterial activity; thus, to promote this functionality an antibacterial agent should be added [10,11].

Presently different antibacterial agents based on organic (e.g. chitosan) and inorganic materials (e.g. Ag; ZnO; TiO_2) are being studied

* Corresponding author at: SEG-CEMMPRE Mechanical Engineering Department, University of Coimbra, 3030-788 Coimbra, Portugal.
E-mail address: uc43448@uc.pt (I. Carvalho).

https://doi.org/10.1016/j.diamond.2018.03.035
Received 9 November 2017; Received in revised form 29 March 2018; Accepted 31 March 2018
Available online 04 April 2018
0925-9635/

with the aim of improving the performance of components and devices susceptible to provoke infections [12]. Among them, Ag has gained a considerable attention due to its high effectiveness in destroying a wide range of microorganisms. Silver coated ureteral catheters, antibiotics based on silver salts for the treatment of burns and leg ulcers, application of silver nitrate solutions against ophthalmia neonatorum are examples of some of the most common uses of this metal in medicine [13]. On the other hand, the advent of nanotechnology has brought the possibility to produce Ag at nano scale, which is claimed to promote huge improvements in the antibacterial efficiency of this metal. The considerable increase in the surface to volume ratio at nanoscale allows obtaining high antimicrobial efficiency, even for small amounts of dopants [12]. Sputtering of Ag-MeN [14], Ag-MeCN [15], Ag-DLC [16] allows to reach a nanocomposite structure, where Ag nanoparticles are dispersed in the matrix. Alloying DLCs with Ag nanoparticles has been a solution for fixing the nanoparticles and allowing silver ions release along the time [17]. However, mechanical and tribological studies of the stent coating play a significant role to achieve the desired functional properties of ureteral stents including flexibility, biocompatibility, corrosion resistance, low friction coefficient, and wettability. Despite the major improvements regarding the development of antibacterial stents, none of the concepts developed are able to fully satisfy the required goals. In this sense, the development of new materials is still an ongoing process, which has attracted a lot of investments and research over the last years [18]. In fact, the shape, size, and distribution of Ag nanoparticles will dictate the in-service behaviour of these coatings which requires a deep control on the production parameters [19]. Therefore, it is essential to study the tribological behaviour of the material used for ureteral stents in order to validate its suitability for the application.

With that purpose, in this study, a magnetron sputtering equipment connected with a homemade gas aggregation clusters source was used to deposit Ag/a:C coating on carbon grid and ureteral stents to investigate the distribution sizes of clusters in a:C matrix and the tribological properties of the coatings, respectively. For that, the agglomeration parameters in the clusters source, the Ag incorporation in the a:C coatings and, also, the deposition parameters on the main chamber were the focus of this study. Then, considering the Ag structural arrangement in the a:C matrix, frictional properties were studied. Counter bodies and lubricants were carefully selected and the human body in-service conditions for the stents were simulated by using an ex-vivo homemade tribotest set-up to evaluate the friction behaviour, as an important factor for this application.

2. Material and methods

2.1. Samples deposition

A magnetron sputtering equipment connected with a gas aggregation cluster source was used to deposit Ag/a:C coating on carbon grids (Monocomp Instrumentación SA), silicon, polyurethane tape, material with which the stents are made (Tecoflex EG93A, Velox - Specialities in Motion) and polyurethane stent (Bard) substrates. Carbon grids were used to evaluate the size distribution of Ag cluster in a:C matrix, the silicon to evaluate the morphology and the cross section, the polyurethane tape for adhesion tests and the polyurethane stent for tribological assays. The gas aggregation cluster source consists in a magnetron head cooled by water, gas supply pipes, an aggregation chamber cooled by water and an orifice through which the clusters are ejected to the deposition chamber. The clusters source is separated from the main chamber by an exit orifice with a diameter of 2 mm. A silver (99.99%, Testbourne Ltd) target with an area of 2000 mm^2 was connected to the magnetron head. In the deposition chamber, a carbon (99.99%, Testbourne Ltd) target with $100 \times 200\ mm^2$ was attached to the cathode. A rotating substrate holder was located 70 mm from both, C target and cluster's exit orifice. The rotation speed of substrate holder was kept constant at 10 rpm to achieve a homogeneous cluster distribution in the a:C matrix. A negative pulsed DC bias voltage of 50 V was applied to the substrate holder and no additional heating was applied. Power density applied to carbon and silver targets was constant at 1.5 $W{\cdot}cm^{-2}$ and 2.5 $W{\cdot}cm^{-2}$, respectively. The Ar gas was introduced through the cluster source to reach the pressure of 100 and 200 Pa in order to produce Ag clusters, which were incorporated in a:C matrixes. An intermediate vacuum system between the clusters source and the main deposition chamber allowed to keep in the latter a constant pressure of 3×10^{-1} Pa. The same deposition parameters were applied to produce the a:C coatings, power density applied to carbon was constant at 1.5 $W{\cdot}cm^{-2}$ and Ar gas was also introduced through the cluster source to reach a work pressure of 3×10^{-1} Pa. The deposition times were adjusted in order to obtain a thickness of 55 nm for the deposition on carbon grids and polyurethane stent substrate and 200 nm for the deposition on silicon and polyurethane tape substrates.

2.2. Morphological analyses

Morphological characterization was achieved by FDSEM, ZEISS MERLIN Compact/VP Compact, while surface roughness was characterized by atomic force microscopy (AFM Brunker Innova system). Scanning Transmission Electron Microscopy (STEM) was performed on Ag/a:C coated carbon grids at a magnification of 50 Kx for clusters produced at 200 Pa and 100 Kx to clusters produced at 100 Pa. The size distribution of Ag clusters in a:C matrix was determined by analysing the STEM micrographs in ImageJ software. Counting of the clusters produced by the pressure at 200 Pa was considered bimodal with a restriction of area size, for smaller clusters below 3000 nm^2 and for aggregates above 3000 nm^2. For the clusters produced by the pressure at 100 Pa, only the restriction of area below 3000 nm^2 was applied. The mean cluster size and standard deviation were also determined from the distribution of the measured feret diameters. Clusters feret diameter distribution was obtained for four micrographs for each sample. Scanning Electron Microscope (SEM) was performed to Ag/a:C coatings to determine the thickness and the deposition rate, the magnification used were 50 Kx and 80 Kx to the topography and cross section, respectively. The roughness measurements were performed using a Brunker Innova system in tapping mode with Si probe with a tip radius of 8 nm. Surface parameters evolution was collected using Gwyddion software after application of the mean plane correction in order to reduce waviness due to scanner bow and variations of the film thickness and line wise levelling to reduce possible line-by-line repetition errors.

In order to estimate the evolution of silver content with time, carbon grids deposited with Ag/a:C coatings were immersed into a vessel containing 2 ml of distilled water at room temperature. The samples were taken out after 2, 24, 48 and 168 h and after drying at room temperature, the STEM images were acquired by FESEM at a magnification of 50 Kx and 100 Kx and analysed in ImageJ software following the procedure above described. For each time, the average mass of Ag clusters in the coatings was estimated as follows: (i) at least 4 images were analysed for each condition; (ii) taking each feret diameter, and considering the particles as spheres, the individual mass of each cluster was calculated from the volume and the Ag density; (iii) the total mass of silver was determined by summing all the clusters masses; (iv) finally, after dividing the mass per the area observed in each micrograph, an average value was determined by considering all the micrographs analysed in each sample.

2.3. Adhesion assay

Adhesion tests were performed according with the standard D 3359 – 97 [20] and the standard ISO 2409:2007 [21]. Both tests are based on the measurement of adhesion with adhesive tape. However, D 3359 – 97 assess the adhesion of coating films to metallic substrates while ISO 2409:2007 is applicable to hard and soft substrates, but only measures

the adhesion of paint or varnishes coatings. As this study has the purpose of coat polyurethane ureteral stent with Ag/a:C films, these two standards were considered since the test was performed to polyurethane tape, a soft substrate coated with Ag/a:C. Both tests are based on drawing a scalpel with horizontal and vertical lines with a spacing of 1 mm. The drawing of this grid should be done under the coated surface in an area with no imperfections and between each stroke, the area should be brushed to avoid scratching the substrate. The tape used for this test has a width of 40 mm and is pressure sensitive. After the grate is drawn, a piece of tape is removed, about twice the length of the sample, and it is extremely important that this piece of tape does not touch any type of material before finishing the test. Thereafter, the tape portion is centred with the sample, and is glued. To ensure uniform adhesion, a rubber is used and gently passed over the adhesive tape adhered to the sample. The adhesive tape is then quickly removed without being pulled out, at an angle as close as possible to 180°. The test was repeated in three other locations on each sample. The images were acquired by an Olympus SZ-CTV Stereo Microscope.

2.4. Ex-vivo tribotest set-up

Fig. 1 describes a scheme of the tribotest device which measures the force required to drag the sample stent, at a known velocity (100 mm·min^{-1}) across the static counter bodies. The sample stent with about 20 cm in length is positioned between two pieces of counter bodies: fresh porcine liver cuts, the outer liver surfaces fronting each other. The porcine liver's outer surface is reported to have comparable friction behaviour as the ureter's endothelial tissue through its particular mucosa and secretory capabilities, and this is because of the outer Tunica serosa, a membrane with a secretory epithelial layer, which produces a thin lubricating serous fluid [22,23]. This ex-vivo tribotest device is preferred over an in-vivo animal model due to acceptable reproducibility of the test as imperative requirements. Additionally loads (D) of 5, 10 and 15 N were used on the covering block in order to adjust the load differences and ensure equal initial loads for various liver slices. The sample stent also was tensioned with a dead weight (G), in order to confine the friction interaction on the sample surface during the test. On the other side, the sample stent was connected to a tensile testing machine (Shimadzu Autograph AG-X) through a lightweight nylon filament over a low friction pulley to record the tractive force required to pull sample stent during the experiment. The experiment was repeated with different compressive loads. Each stent sample was measured threefold under each particular load in order to acquire a statistically valid number of data. Two new stent samples were used for each load. Moreover, the same procedure was repeated for the uncoated reference stents. For each sample, fresh liver cuts were used. The samples and counter bodies were completely soaked in 0.9% saline solution for 60 min before the measurements to guarantee uniform prewetting of the test surfaces. Also, the specimens were lubricated with 0.9% saline solution during test operation.

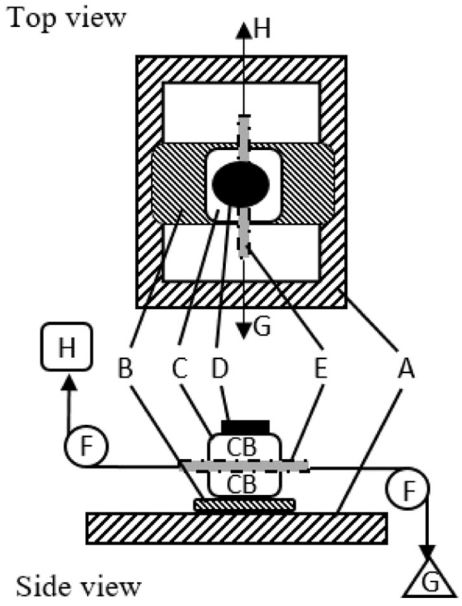

Fig. 1. Schematic of the experimental set-up, the ex-vivo tribotest device, used to determine the apparent friction coefficient. A – holding frame; B – plastic plate; C – a vessel containing counter body; CB – exchangeable counter body; D – covering block for load; E – stent sample; F – low friction pulley; G – dead weight; H – tractive force by a tensile testing machine.

3. Results

3.1. Morphological study

The clusters size was evaluated by analysing the STEM images. STEM images are depicted in Figs. 2 and 3 together with the clusters size distribution histograms for the deposition of Ag/a:C with the pressure of cluster source at 100 and 200 Pa, respectively. A huge difference can be found in the cluster mean size, when the clusters are produced with pressure at 100 Pa, the value is 11 ± 2 nm (Fig. 2a), while for the clusters produced with pressure at 200 Pa, a bimodal size is observed; the mean size of smaller clusters is 31 ± 22 nm (Fig. 3a) and the mean size for the aggregates is 260 ± 135 nm (Fig. 3a$_1$).

Figs. 2 and 3 also show the evaluation of clusters size distribution over the immersion time of samples in distilled water, b) after 24 h and c) after 168 h, (data for 2 h and 48 h after immersion are similar to data for 24 h, not shown). For Ag clusters produced with the pressure of 100 Pa, only small changes were observed over the immersion time, particularly in the initial stage of immersion (up to 2 h). Moreover, a closer analysis of the histogram allows to conclude that the relative intensity of smaller diameters increases (compare e.g. the 3rd/4th and the 2nd/3rd bars from the left between as-deposited/24 h and 24 h/168 h, respectively). For the samples with Ag clusters produced at 200 Pa, a much stronger decrease of the mean size of both aggregates and isolated nanoparticles are observed. Again, the decrease is much faster in the first 2 h of immersion (from 31 down to 27 and 260 down to 205 nm for agglomerate and isolated nanoparticles, respectively) than thereafter (see values for 24 and 168 h in Fig. 3). Sporadically, big clusters (Fig. 3b$_1$ and c$_1$ in black) are detected which after 7 days (Fig. 3c$_1$) of immersion become smaller. In all these cases the size reduction can be attributed to the release of Ag to the media, as demonstrated by the decrease in the average mass of Ag clusters as shown in Fig. 4.

Fig. 5 shows the surface morphology of the pure a:C and Ag/a:C coatings. The topographic images show a homogenous distribution of top domes over the surface for both Ag/a:C depositions, related to the columnar structure observed in cross section (see insets in Fig. 5b and c). The pure a:C coating shows also a columnar structure (see inset in Fig. 5a) but more compact with a much smoother surface (see Fig. 5a) suggesting that the presence of Ag nanoparticles creates new nucleation sites interfering with the normal growth of the a:C matrix. Ag nanoparticles are difficult to be identified in 100 Pa deposited samples but are clearly seen in surface view for the 200 Pa depositions (bright dots in Fig. 5c). Fig. 6 shows AFM images of the samples surface as well as the roughness values for the a:C and Ag/a:C coatings. With the addition of Ag cluster to a:C matrix, an increase in the roughness is observed corroborating the SEM analysis.

3.2. Adhesion test

Fig. 7 shows the optical microscope image of the surface of the coated polyurethane tape samples before adhesion tests (a, b and c) and after adhesion tests (a$_1$, b$_1$, c$_1$). Fig. 7a$_2$, b$_2$ and c$_2$, also show grated

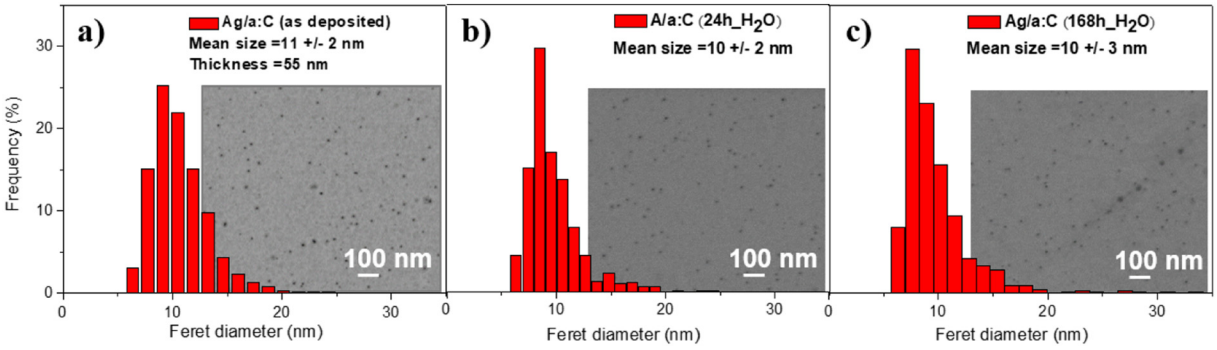

Fig. 2. Feret distribution histograms of Ag cluster in a:C matrix at 100 Pa, a) as deposited, b) and c) after of 24 h and 168 h immersion in distilled water, respectively. STEM micrographs at magnification of 100 Kx in insets.

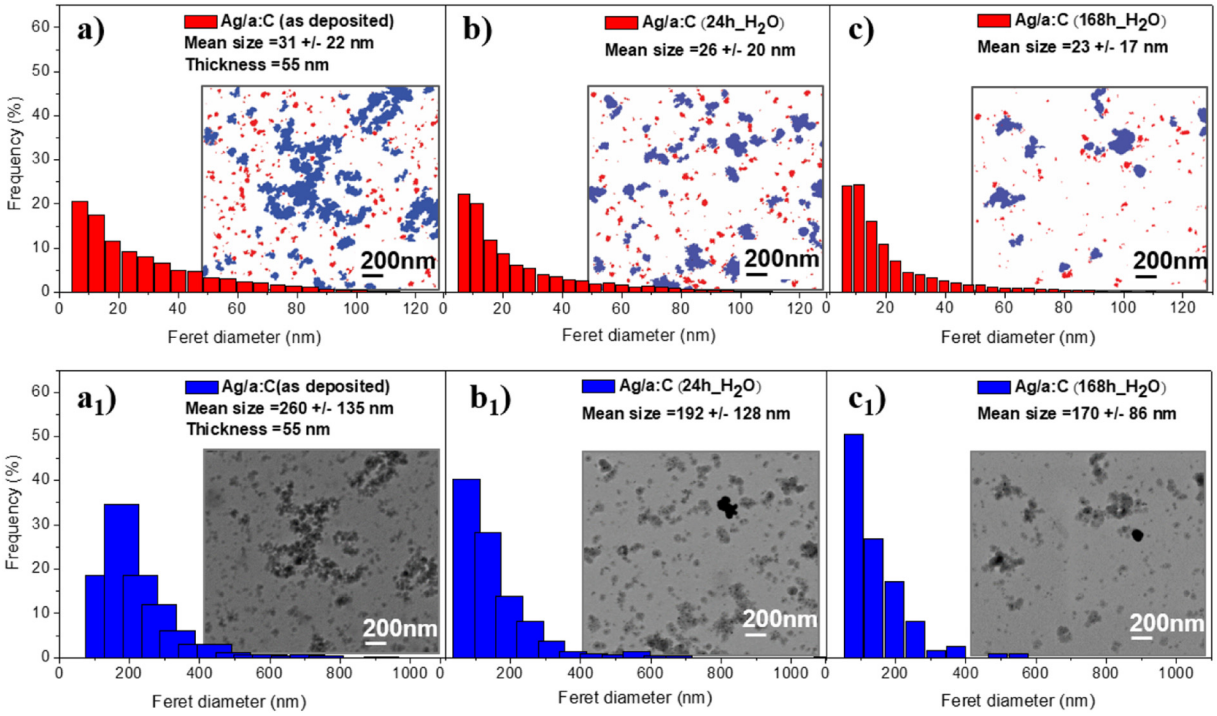

Fig. 3. Feret distribution histograms of Ag cluster in a:C matrix at 200 Pa, a) and a_1) as deposited, b) and b_1) after 24 h of immersion in distilled water, and c) and c_1) after 168 h of immersion. STEM micrographs at magnification of 50 Kx in insets, the blue bars correspond to aggregate and the red ones correspond to the individual clusters. (For interpretation of the references to color in this figure legend, the reader is referred to the web version of this article.)

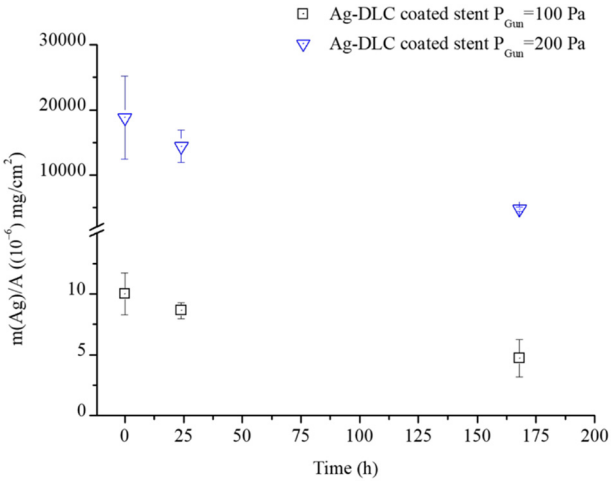

Fig. 4. Ag cluster mass in a:C matrix per area unit vs. immersion time in distilled water.

samples after being immersed in distilled water during one month and then submitted to the adhesion tests. Fig. 7a, b and c refer to a:C, a:C with clusters produced at 100 Pa and a:C with clusters produced at 200 Pa.

For all depositions, none of the squares of the network is detached. The edges of the cuts are completely smooth, suggesting an excellent adhesion, at least in accordance to the ISO 2409:2007 standard definitions.

3.3. Ex-vivo friction behaviour

The homemade developed tribotest device allows to measure the apparent coefficient of friction between the sample stent and the tissue simulating counter bodies. According to the Amonton-Coulomb friction rule, a simple force equilibrium can provide the friction coefficient from the Eq. (1):

$$\mu = \frac{F_s}{F_w} \quad (1)$$

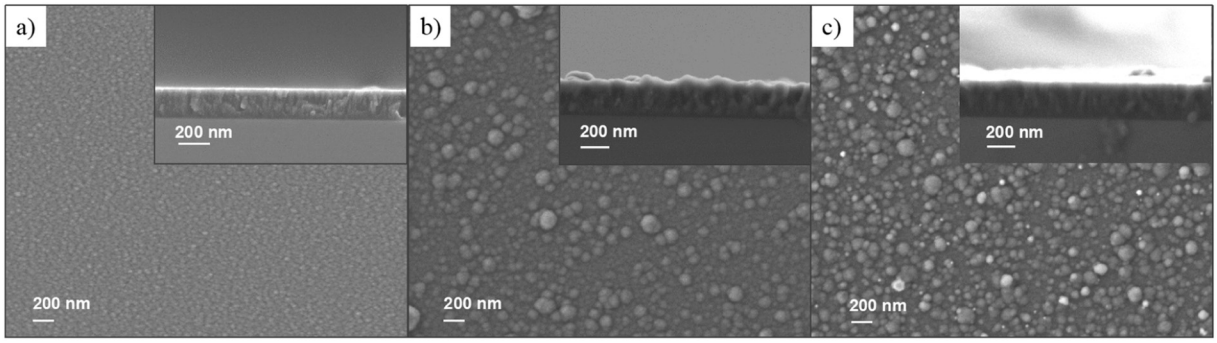

Fig. 5. SEM micrograph of pure a:C coating a) and Ag/a:C coating b) at 100 Pa and c) at 200 Pa at a magnification of 50 Kx, in inset the cross section at a magnification of 80 Kx.

where, F_s indicates the traction force applied to drag the sample stent, during the instant motion, and F_w the normal load exerted on the sample stent.

Fig. 8 shows a typical tractive force versus path diagram (mean values of forces measured within three runs) of the a:C, Ag/a:C (with clusters produced at 100 and 200 Pa) coated and uncoated stents, acquired with the 5 N applied normal load. Under the same experimental conditions, the tractive forces required to drag the coated stents are significantly less than the reference stent. The experiment was repeated with different compressive loads. The force required to maintain a continuous movement under different normal loads for the a:C and Ag/a:C coated stents as well as the reference stent is shown in Fig. 9. The apparent coefficient of frictions determined from the slope of the trendlines is presented in Table 1. It can be seen that the friction coefficient varied from 0.22 ± 0.03 for the reference stent to 0.10 ± 0.01 for the a:C coated stent, to 0.12 ± 0.02 for the Ag/a:C coated stent with clusters produced at 100 Pa and to 0.16 ± 0,01 for the Ag/a:C coated stent with clusters produced at 200 Pa.

4. Discussion

The increase in clusters size with the pressure in the cluster source is due to the increase of the collisions probability in the gaseous phase between Ar, metal atoms and clusters leading to either the direct (aggregation) or indirect (increasing of the time a cluster remains within the growth region) increase in cluster size. After immersion in distilled water a decrease in the mean size of the clusters/aggregates were observed for both coatings containing Ag clusters produced with 100 and 200 Pa, particularly in the first times of immersion. As it was shown in a previous work [10] the diffusion of Ag in a:C coatings is only possible if Ag nanoparticles are in the surface or in columns boundaries. Therefore, the release of Ag to the aqueous media can only occur from the nanoparticles that are in direct contact with the water. After the first Ag release, the nanoparticles in those conditions reduce their size and the exposed area decreases, with the consequent decrease in the nanoparticles size. This process should proceed up to the complete vanishing of the nanoparticles. It should be remarked that the variation in the mean value displayed in Fig. 2 is very small, particularly for 100 Pa sample, since the mean value calculation is integrating all the nanoparticles embedded in the C:based matrix from which no Ag is released. The decrease much more pronounced in the 200 Pa sample than for 100 Pa should be related with the bigger dimension of the clusters in the former. The thickness of the coating is only close to 50 nm, which means that there will be a significant amount of nanoparticles that can be almost out of the matrix (nanoparticles mean size is > 30 nm in the as-deposited conditions) not embedded in the C:based matrix. The formation of big clusters is a consequence of the clusters mobility on the samples surface which, as shown in a previous work, can lead to a coalescence process based on a dissolution/reprecipitation mechanism [24]. The control of silver release from the a:C matrix is a very important step to promote antimicrobial properties without causing any allergic reaction to the biomaterial in study, i.e. the stent coated with Ag/a:C. The loss of Ag mass verified in the coatings over the immersion time shows that silver is being released. For this reason, the availability of silver in the electrolyte shows the potential of these coatings to combat microbial infections. More studies are needed, namely using inductively coupled plasma optical emission spectrometry (ICP-OES), to determine the release of silver in the electrolyte.

The adhesion of the coatings to the polyurethane tape is excellent since no delamination, peeling or flaking was observed in any of the zones of the coated surfaces, even in the borders of the grooves created by the cutting knife.

In tribology results, the peak observed at the beginning of the stent movement refers to the maximum value of the coefficient of friction (COF), denominated static COF. When the stent keeps moving, the recorded value is lower, describing the kinetic COF. A significant reduction of the COF values could be registered, from 0.22 ± 0.03 of the uncoated stent down to 0.10 ± 0.004, 0.12 ± 0.02 and 0.16 ± 0.01 for a:C, Ag/a:C coated stents with cluster formed at source pressure of 100 and 200 Pa, respectively. From tribological point of view, the a:C

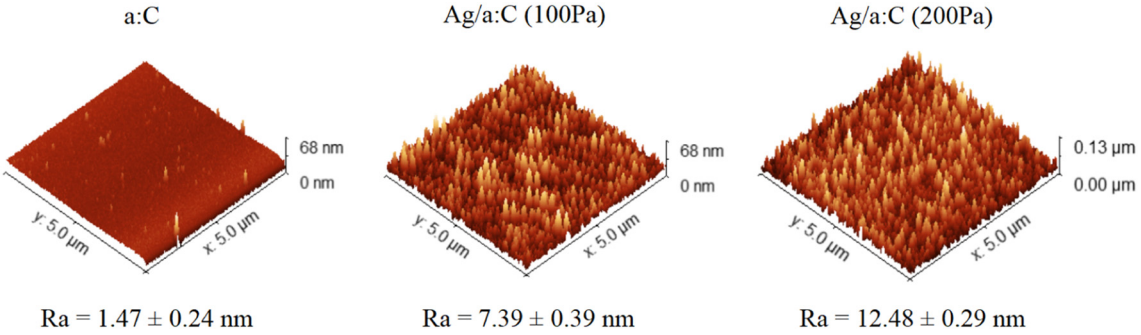

Fig. 6. AFM images of coatings with a scan range of 5 × 5 µm. Ra is the arithmetic mean values of the surface roughness.

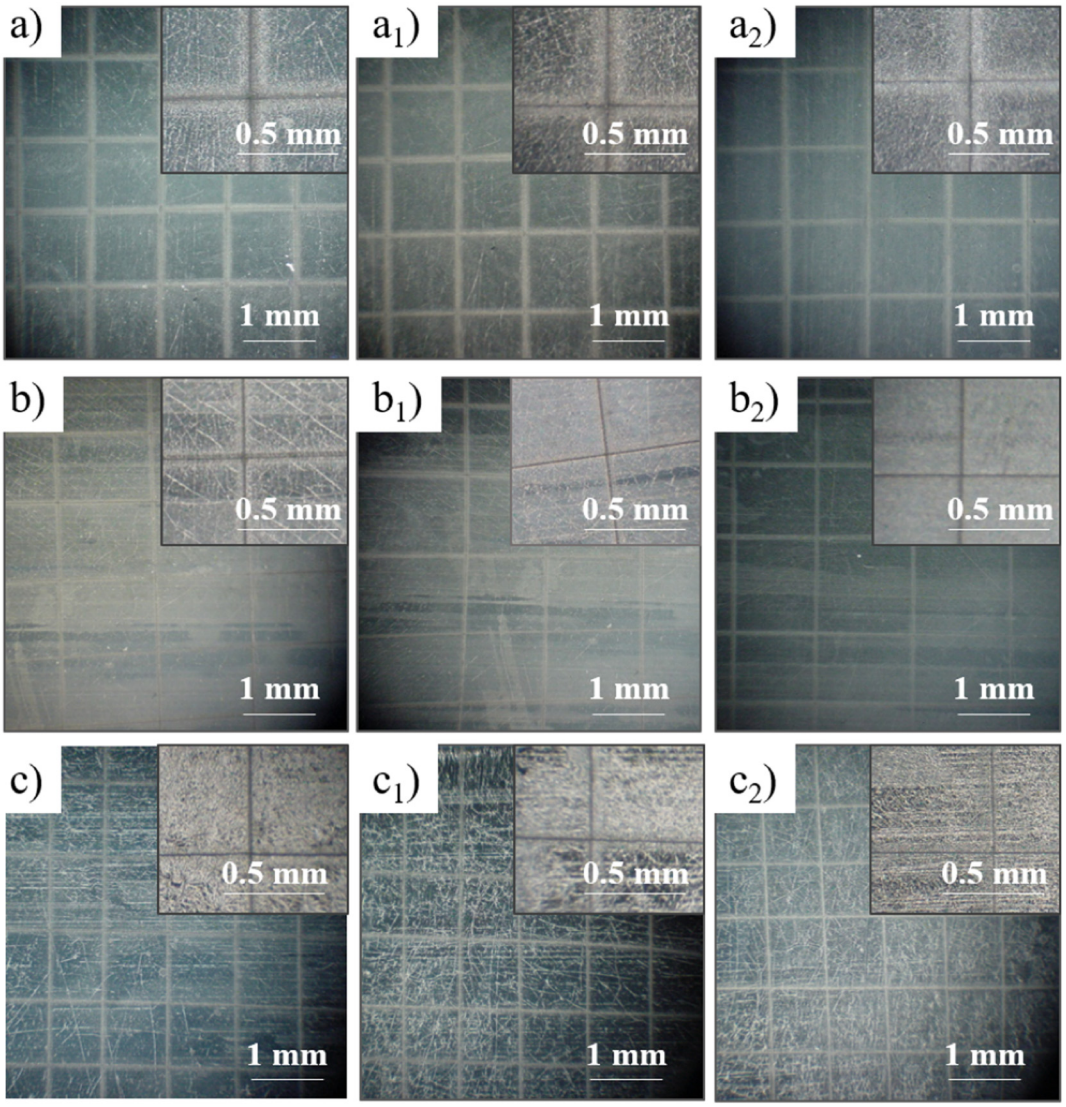

Fig. 7. Optical microscopy images of a:C and Ag/a:C coatings, a), b) and c) before and a_1), b_1) and c_1) after adhesion tests, a_2), b_2) and c_2) after one month of immersion in distilled water a), a_1) and a_2) at 100 Pa and b), b_1) and b_2) at 200 Pa. c), c_1) and c_2) referring to a:C.

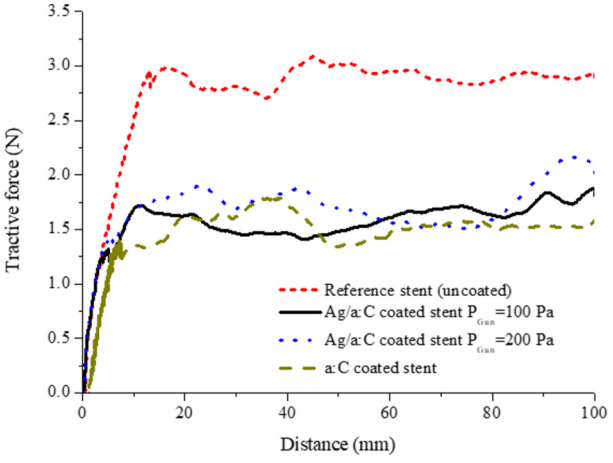

Fig. 8. Typical plot showing a distance vs. tractive force obtained with the applied normal load equal to 5 N from the measurements with the ex-vivo tribotest.

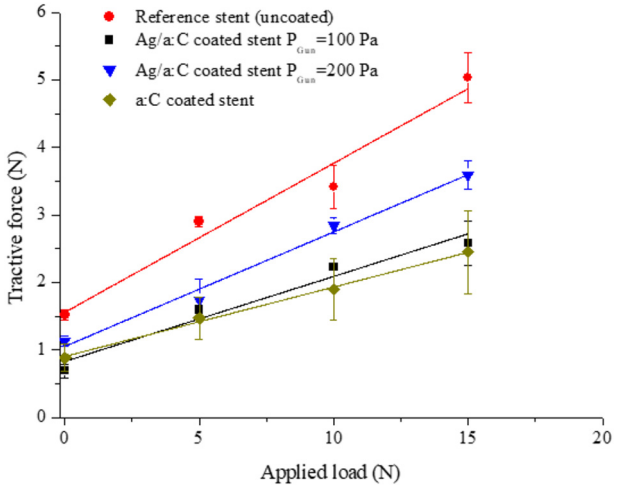

Fig. 9. Tractive force vs. applied load for Ag/a:C coated stents and uncoated reference.

Table 1
The apparent coefficient of friction.

Sample	Apparent COF
a:C coated stent	0.10 ± 0.004[b]
Ag/a:C coated stent [a]P_{Gun} = 100 Pa	0.12 ± 0.02
Ag/a:C coated stent P_{Gun} = 200 Pa	0.16 ± 0.01
Reference stent (uncoated)	0.22 ± 0.03

[a] Cluster source pressure.
[b] Standard error.

and 100 Pa samples give lower friction coefficient, which should be related to either their lower surface roughness (no protuberances induced by the clusters in the case of a:C) or to Ag/a:C the lower area of contact with Ag surface (smaller clusters in the case of Ag/a:C produced with 100 Pa when compared to those produced at 200 Pa). The lower friction coefficient in stents facilitates the insertion or removal of the device during the operation and minimize irritation and abrasion of the ureter tissues which would in turn decrease the possibility of submucosal inflammation and infection. These results show that a:C and Ag/a:C produced at 100 Pa have a better behaviour in terms of tribological performance: however, it should be noted that one of the causes of stent failure is the bacterial colonization. In a previous study [10] we proved that a:C coatings did not show antibacterial activity, which makes them not suitable for these applications. Silver can be the needed as antibacterial agent which makes these Ag/a:C coatings a potential solution for the stents application. Further studies concerning biological behaviour are now needed to evaluate the cytotoxicity and antimicrobial properties of these coatings.

5. Conclusion

Polyurethane stent and tape as well as carbon grid substrates were coated with a:C and Ag/a:C films (Ag clusters embedded in a:C matrix) by using a magnetron sputtering equipment connected to a homemade cluster source.

The mean sizes achieved by varying the cluster source pressure were 11 ± 2 nm, at 100 Pa and a bimodal mode of 31 ± 22 nm and 260 ± 135 nm at 200 Pa. When immersed in distilled water, Ag release for the media was observed, in higher quantities for either the initial times of immersion for samples which clusters were growth with 200 Pa.

The homemade tribotest device developed for this work allowed ex-vivo studies of the tribological characterization of the stents, in a convenient, fast, reproducible and objective way. The proposed set-up mimics the in-vivo conditions during stenting due to presence of saline solution (body fluid) and a tissue as a counter body. The results for the kinetic friction coefficient show the great difference between the coated and uncoated stents, with a decreasing of 45%, which confirm the benefit influence of the coating on the friction behaviour of the stent promising a facile handling. This is extremely important for the patient comfort after insertion reducing pain, one of the first key factors in developing new materials for using as stent.

Acknowledgments

The authors thankfully acknowledge financial support by Erasmus Mundus MSc course TRIBOS – Joint European Mater in Tribology of Surface and Interfaces – 532535-1-SI-2012-1-ERA MUNDUS-EMMC and Portuguese national funds through FCT-Fundação para a Ciência e a Tecnologia, under the project PTDC/CTM-NAN/4242/2014, “Clusters bimetálicos para ação antimicrobiana controlada em stents”, projeto MATIS - Materiais e Tecnologias Industriais Sustentáveis (CENTRO-01-0145-FEDER-000014) and ERA-SIINN/0004/2013 project.

References

[1] D. Lange, S. Bidnur, N. Hoag, B.H. Chew, Ureteral stent-associated complications—where we are and where we are going, Nat. Rev. Urol. (2014), http://dx.doi.org/10.1038/nrurol.2014.340.
[2] L. Yang, S. Whiteside, P.A. Cadieux, J.D. Denstedt, Ureteral stent technology: drug-eluting stents and stent coatings, Asian J. Urol. 2 (2015) 194–201, http://dx.doi.org/10.1016/j.ajur.2015.08.006.
[3] N. Laube, L. Kleinen, J. Bradenahl, A. Meissner, Diamond-like carbon coatings on ureteral stents-a new strategy for decreasing the formation of crystalline bacterial biofilms? J. Urol. 177 (2007) 1923–1927, http://dx.doi.org/10.1016/j.juro.2007.01.016.
[4] J.P. Burke, Infection control—a problem for patient safety, N. Engl. J. Med. 348 (2003) 651–656, http://dx.doi.org/10.1056/NEJMhpr020557.
[5] D.R. Monteiro, L.F. Gorup, A.S. Takamiya, A.C. Ruvollo-Filho, E.R. de Camargo, D.B. Barbosa, The growing importance of materials that prevent microbial adhesion: antimicrobial effect of medical devices containing silver, Int. J. Antimicrob. Agents 34 (2009) 103–110, http://dx.doi.org/10.1016/j.ijantimicag.2009.01.017.
[6] P. Tenke, C.R. Riedl, G.L. Jones, G.J. Williams, D. Stickler, E. Nagy, Bacterial biofilm formation on urologic devices and heparin coating as preventive strategy, Int. J. Antimicrob. Agents (2004), http://dx.doi.org/10.1016/j.ijantimicag.2003.12.007.
[7] K. Enomoto, T. Hasebe, R. Asakawa, A. Kamijo, Y. Yoshimoto, T. Suzuki, K. Takahashi, A. Hotta, Controlling the drug release rate from biocompatible polymers with micro-patterned diamond-like carbon (DLC) coating, Diam. Relat. Mater. 19 (2010) 806–813, http://dx.doi.org/10.1016/j.diamond.2010.01.053.
[8] B.H. Chew, M. Duvdevani, J.D. Denstedt, New developments in ureteral stent design, materials and coatings, Expert Rev. Med. Devices 3 (2006) 395–403, http://dx.doi.org/10.1586/17434440.3.3.395.
[9] D. Lange, B.H. Chew, Update on ureteral stent technology, Ther. Adv. Urol. 1 (2009) 143–148, http://dx.doi.org/10.1177/1756287209341306.
[10] N.K. Manninen, S.V. Calderon, I. Carvalho, M. Henriques, A. Cavaleiro, S. Carvalho, Antibacterial Ag/a-C nanocomposite coatings: the influence of nano-galvanic a-C and Ag couples on Ag ionization rates, Appl. Surf. Sci. 377 (2016), http://dx.doi.org/10.1016/j.apsusc.2016.03.113.
[11] L.J. Wang, F. Zhang, A. Fong, K.M. Lai, P.W. Shum, Z.F. Zhou, Z.F. Gao, T. Fu, Effects of silver segregation on sputter deposited antibacterial silver-containing diamond-like carbon films, Thin Solid Films 650 (2018) 58–64, http://dx.doi.org/10.1016/j.tsf.2018.02.015.
[12] Q. Li, S. Mahendra, D.Y. Lyon, L. Brunet, M.V. Liga, D. Li, P.J.J. Alvarez, Antimicrobial nanomaterials for water disinfection and microbial control: potential applications and implications, Water Res. 42 (2008) 4591–4602, http://dx.doi.org/10.1016/j.watres.2008.08.015.
[13] J.M. Schierholz, L.J. Lucas, A. Rump, G. Pulverer, Efficacy of silver-coated medical devices, J. Hosp. Infect. 40 (1998) 257–262.
[14] H.-L. Huang, Y.-Y. Chang, M.-C. Lai, C.-R. Lin, C.-H. Lai, T.-M. Shieh, Antibacterial TaN-Ag coatings on titanium dental implants, Surf. Coat. Technol. 205 (2010) 1636–1641, http://dx.doi.org/10.1016/j.surfcoat.2010.07.096.
[15] P.J.J. Kelly, H. Li, P.S.S. Benson, K.A.A. Whitehead, J. Verran, R.D.D. Arnell, I. Iordanova, Comparison of the tribological and antimicrobial properties of CrN/Ag, ZrN/Ag, TiN/Ag, and TiN/Cu nanocomposite coatings, Surf. Coat. Technol. 205 (2010) 1606–1610, http://dx.doi.org/10.1016/j.surfcoat.2010.07.029.
[16] N.K. Manninen, R.E. Galindo, N. Benito, N.M. Figueiredo, A. Cavaleiro, C. Palacio, S. Carvalho, Ag–Ti(C, N)-based coatings for biomedical applications: influence of silver content on the structural properties, J. Phys. D. Appl. Phys. 44 (2011) 375501, , http://dx.doi.org/10.1088/0022-3727/44/37/375501.
[17] M. Cloutier, S. Turgeon, Y. Busby, M. Tatoulian, J.J. Pireaux, D. Mantovani, Controlled distribution and clustering of silver in Ag-DLC nanocomposite coatings using a hybrid plasma approach, ACS Appl. Mater. Interfaces (2016), http://dx.doi.org/10.1021/acsami.6b06614.
[18] J.S. Lam, M. Gupta, Update on ureteral stents, Urology 64 (2004) 9–15, http://dx.doi.org/10.1016/j.urology.2004.03.005.
[19] N.K. Manninen, N.M. Figueiredo, S. Carvalho, A. Cavaleiro, Production and characterization of Ag nanoclusters produced by plasma gas condensation, Plasma Process. Polym. 11 (2014) 629–638, http://dx.doi.org/10.1002/ppap.201300175.
[20] M.P. Dispenser, Standard Test Methods for, Annu. B. ASTM Stand, i (2005), pp. 1–2, http://dx.doi.org/10.1520/C0471M-16.
[21] EN ISO 2409, Paints and Varnishes, Cross-cut Test, 3 (2013), pp. 4–13, http://dx.doi.org/10.1007/s11367-011-0297-3.
[22] L. Kleinen, U. Böde, N. Laube, Ex-vivo investigations on the friction behavior of amorphous carbon coated ureteral stents, Diam. Relat. Mater. (2008), http://dx.doi.org/10.1016/j.diamond.2008.01.099.
[23] K. Kazmierska, M. Szwast, T. Ciach, Determination of urethral catheter surface lubricity, J. Mater. Sci. Mater. Med. (2008), http://dx.doi.org/10.1007/s10856-007-3339-4.
[24] N.K. Manninen, R.E. Galindo, S. Carvalho, A. Cavaleiro, Silver surface segregation in Ag-DLC nanocomposite coatings, Surf. Coat. Technol. 267 (2015) 90–97, http://dx.doi.org/10.1016/j.surfcoat.2014.12.029.